Monocrystalline Nanopatterns Made by Nanocube Assembly and Epitaxy

*B. Sciacca, A. Berkhout, B. J. M. Brenny, S. Z. Oener, M. A. van Huis, A. Polman, and E. C. Garnett**

Monocrystalline materials are essential for optoelectronic devices such as solar cells, LEDs, lasers, and transistors to reach the highest performance. Advances in synthetic chemistry now allow for high quality monocrystalline nanomaterials to be grown at low temperature in solution for many materials; however, the realization of extended structures with control over the final 3D geometry still remains elusive. Here, a new paradigm is presented, which relies on epitaxy between monocrystalline nanocube building blocks. The nanocubes are assembled in a predefined pattern and then epitaxially connected at the atomic level by chemical growth in solution, to form monocrystalline nanopatterns on arbitrary substrates. As a first demonstration, it is shown that monocrystalline silver structures obtained with such a process have optical properties and conductivity comparable to single-crystalline silver. This flexible multiscale process may ultimately enable the implementation of monocrystalline materials in optoelectronic devices, raising performance to the ultimate limit.

The performance of optoelectronic, plasmonic, and nanophotonic devices depends ultimately on the quality of the materials employed; monocrystalline materials represent the best option to bring the capabilities of such devices to the limit.[1–5] Epitaxy from a lattice-matched substrate or seeded growth from the melt are the main strategies that are routinely employed to make continuous monocrystalline materials with an arbitrary geometry. These approaches require high vacuum, high temperature, or both, constraining the range of materials and device geometries that can be practically achieved.[6] This calls for a more general approach to widen substantially the toolbox of monocrystalline materials available to be employed in devices.

Advances in synthetic chemistry now allow for high-quality monocrystalline nanomaterials at low temperature via solution processing techniques such as colloidal synthesis and oriented attachment, for a multitude of metals, semiconductors, and insulators.[7–13] However, such bottom-up techniques offer limited possibilities to achieve extended structures with control over the final 3D geometry, restricting the use of high quality nanomaterials to niche applications. Here, we present a fundamentally new paradigm to make monocrystalline nanopatterns, which removes the dependence on substrate epitaxy and instead relies on epitaxy between monocrystalline nanocube building blocks. The nanocubes are assembled in a predefined pattern and then epitaxially connected at the atomic level by chemical growth in solution, to form monocrystalline nanopatterns on arbitrary substrates. As a first demonstration, we show that monocrystalline silver structures obtained with such a process have optical properties and conductivity comparable to single-crystalline silver.

The nanowire shape was chosen because it provides a simple platform for measuring conductivity and optical properties, but our new approach to make monocrystalline materials is not limited to nanowire shapes. Instead it is compatible with arbitrary nanoscale patterns that can be assembled in polydimethylsiloxane (PDMS), as has been previously demonstrated in the literature.[14] We chose to use silver for this proof of concept study because it is one of the most studied materials for making monodispersed nanocubes and also has direct implications in the fields of plasmonics, nanophotonics, and optoelectronics. Furthermore, it has many chemical similarities to other metals such as copper, which is extremely important in the microelectronics industry. Semiconductors and dielectrics will certainly be more challenging to realize, but in principle can also be made

B. Sciacca, A. Berkhout, B. J. M. Brenny, S. Z. Oener, A. Polman, E. C. Garnett
Center for Nanophotonics
AMOLF Science Park 104, 1098, XG, Amsterdam, The Netherlands
M. A. van Huis
Debye Institute for Nanomaterials Science
Utrecht University
Princetonplein 5, 3584, CC, Utrecht, The Netherlands
M. A. van Huis
NCHREM
Kavli Institute of Nanoscience
Delft University of Technology
Lorentzweg 1, 2628, CJ, Delft, The Netherlands
Correspondence to: E. C. Garnett (E-mail: garnett@amolf.nl)

DOI: 10.1002/adma.201701064

with this process for materials that can be synthesized colloidally as nanocubes. In that case, this flexible multiscale process could be implemented for monocrystalline materials in optoelectronic devices, raising performance to the ultimate limit.

Figure 1 gives an overview of the process we have developed to make monocrystalline nanopatterns. First, monocrystalline nanocubes are synthesized in solution, purified, and resuspended to make a colloidal ink. Colloidal synthesis of a wide range of metal, semiconductor, and dielectric nanocubes has been reported previously;[9,15–21] here we use 70 nm {100}-faceted silver nanocubes to demonstrate the concept. These nanocubes are assembled into nanoscale trenches patterned in a flexible PDMS template (Figure 1A). The evaporation of the liquid in a receding meniscus drives a flow of nanoparticles toward the contact line, where the nanoparticles accumulate and are trapped by geometrical confinement in the trenches as the solvent evaporates.[22,23] Although we use patterned PDMS, nanoparticle assembly has also been carried out on unpatterned substrates to make close-packed films either by dipcoating or using a Langmuir–Blodgett trough.[24,25] Second, the assembled nanocubes are transferred by contact printing from the PDMS to a new substrate such as silicon, glass, or a transmission electron microscope (TEM) membrane (Figure 1B), with excellent pattern fidelity. This is consistent with previous literature showing that highly complex patterns can be transferred with >95% yield and better than 100 nm positional accuracy.[14] Third, adjacent nanocubes are bridged at the atomic level by the growth of epilayers from a liquid solution at room temperature, with a process that we call "chemical welding." This leads to extended monocrystalline thin wires (Figure 1C,D), in a similar fashion to the Volmer–Weber growth and coalescence of 2D islands on a surface.

Figure 1E shows a scanning electron microscopy (SEM) image of a line of 50 silver nanocubes packed closely together after transfer printing onto a silicon substrate. The excellent assembly occurs due to (i) the intrinsic geometrical symmetry of the nanocubes, (ii) the strong van der Waals attraction between their flat {100}facets, and (iii) the tight confinement provided by an accurate design of the master—the width of the trenches can fit only one nanocube, and in a single orientation, the (100) direction. As a result, the nanocubes are all aligned in the same crystallographic orientation, which is necessary to achieve monocrystallinity after welding. Chemical welding leads to a continuous silver nanowire (Figure 1F). This occurs by epitaxial growth in the sub-1 nm gap between adjacent nanocubes. The contrast visible in the SEM image is due to slight variations in the surface topography. The chemical welding procedure consists of a chemical reaction similar to that employed to synthesize the nanocubes, but under conditions (temperature and concentration) that preclude homogeneous nucleation. In the case of metals, this typically involves the reduction of metal ions, where the nanocube surface acts as a seed for heterogeneous nucleation. Here, we have used a chemical welding solution consisting of an aqueous diamminesilver(I) complex with glucose as the reducing reagent.[26] The process takes 90 s at room temperature. A pretreatment with sodium borohydride was found to be helpful in improving reproducibility, presumably by removing excess polyvinylpyrrolidone that remained on the nanocube surface after the synthesis. To release the stress formed at the interfaces due to slight nanocube misalignment, a very short rapid thermal annealing (RTA) treatment (5 s) was used. Note that rounding of the nanowire ends occurs as a consequence of the RTA treatment. Full details of the process are given in the Supporting Information and results of different welding conditions with and without RTA are reported in Figure S1 (Supporting Information).

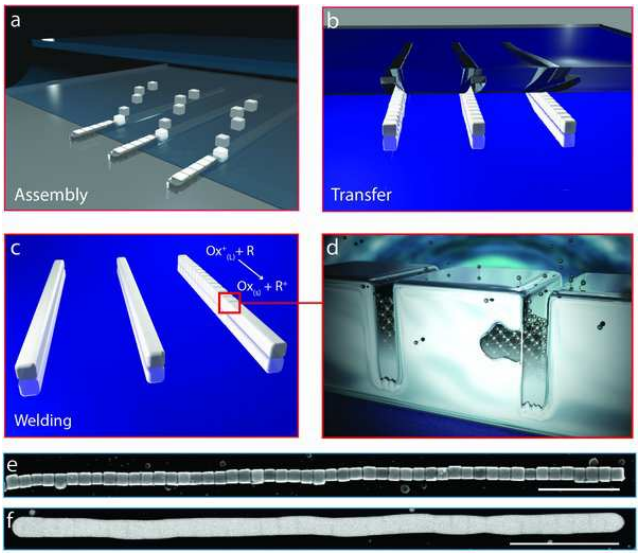

Figure 1. Diagram of the process presented. A) Direct assembly from solution of nanocubes into trenches patterned in a PDMS mold. B) Transfer of the assembled nanocubes to a new substrate. C) Epitaxial welding of the nanocubes into a patterned monocrystalline material via solution processing. D) Artistic representation of the epitaxial nanowelding process. E) SEM image of silver nanocubes on a silicon substrate before and F) after chemical welding. The scale bars are 500 nm.

The assembled nanocubes act as seeds for epitaxial growth of silver adatoms from solution; since the nanocubes share the same crystallographic orientation, this homoepitaxial growth then leads to extended monocrystalline structures. Note that this approach is substantially different from previous reports, which obtained epitaxial attachment of stochastically assembled nanocrystals via simple removal of the surface ligands.[27,28] Here, nanocubes are first assembled in a desired geometry and then exposed to a chemical reaction that provides the material to fill the subnanometer gaps. This key difference makes our approach more broadly applicable, for example, to materials with low atomic mobility and to imperfect assemblies where adjacent nanocubes are separated by larger distances.

Figure 2A (center image) shows a TEM overview of an assembly of four adjacent nanocubes after welding, lying on a thin Si_3N_4 membrane. The segment looks very homogeneous, and the original position of the nanocubes (before welding) can only be inferred from the geometry; the dashed lines superimposed on the image indicate the expected original location of the nanocubes. High resolution TEM (HRTEM) images were taken for the three interfaces—top (TI) and bottom (BI)—at locations corresponding to original interfaces between nanocubes, as indicated by the white squares in Figure 2A. The lattice-resolved images display no sign of interfaces, but a continuous crystal

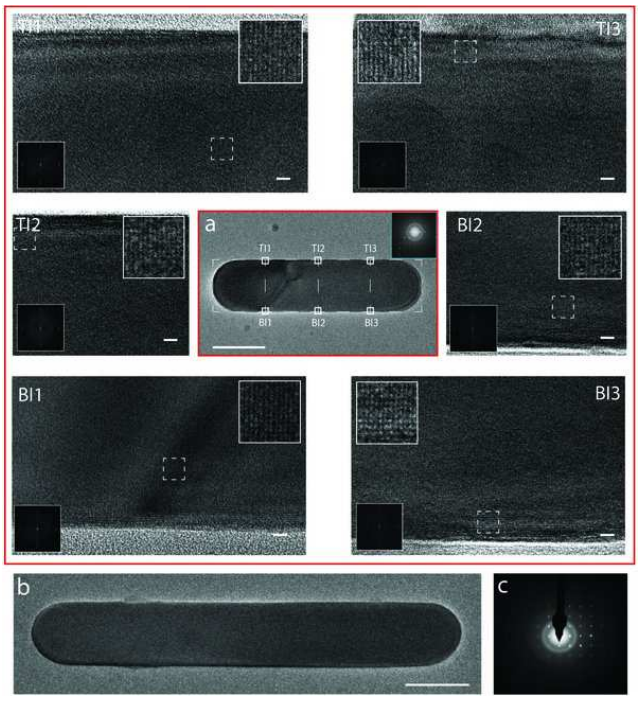

Figure 2. TEM images of welded silver nanocube lines. A) Overview image (center) surrounded by six high-resolution magnifications TI1–3 (top interfaces) and BI1–3 (bottom interfaces) of a bar originally composed of four silver nanocubes; the dashed lines in (A) indicate the location of the nanocubes before welding; the solid squares in a indicate the locations where the HRTEM images were taken, at the expected locations of the interfaces; the inset in (A) represent the SAED pattern of the entire welded line. The insets presented in the HRTEM images show magnified areas corresponding to the dashed squares (top inset) and the respective Fourier Transforms of the entire images (bottom inset). B) TEM image of seven welded nanocubes and C) its SAED pattern showing monocrystallinity on the full scale. The scale bars are 75 nm for TEM images (A, B) and 2 nm for HRTEM images.

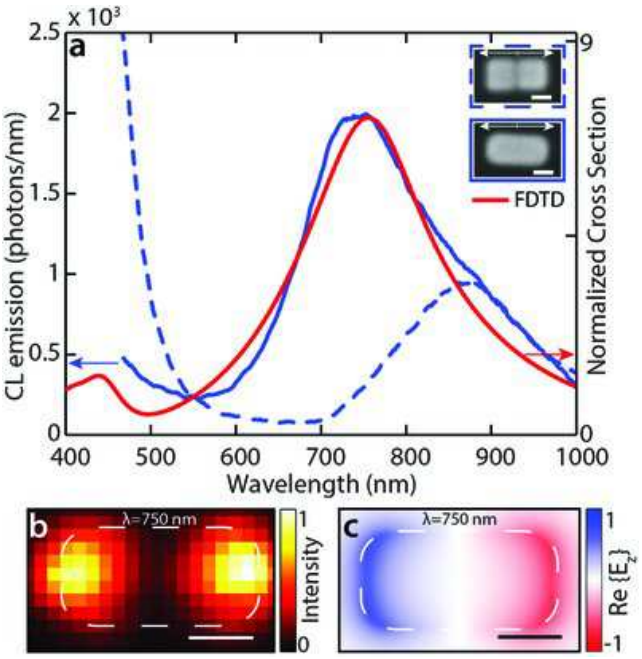

Figure 3. Optical characterization via CL. A) Measured CL spectra of a dimer before (dashed line) and after (solid blue line) welding; the insets show the SEM images. The red line represents the scattering spectrum normalized by the geometrical cross section of a welded dimer, computed by FDTD. For all curves the polarization is parallel to the long axis of the dimer. B) Normalized 2D CL map for the welded dimer measured at $\lambda = 750$ nm, integrated over a 30 nm bandwidth. C) Simulated 2D field profile of the real part of the E_z electric field at $\lambda = 750$ nm for a welded dimer of comparable size, indicating a dipolar mode; the distribution was taken at half-height of the dimer. All scale bars are 50 nm.

lattice in all directions, for every location analyzed. The bottom insets in the HRTEM images are the Fourier transforms of the entire image and indicate the presence of only one lattice period (2.04 Å), corresponding to the {200}lattice spacing for silver. The top insets are taken at higher magnification and clearly resolve the atomic columns.

The inset in Figure 2A (center) shows the selected area electron diffraction (SAED) pattern for the entire line, corresponding to a single [100]-oriented face-centered cubic (fcc) lattice. These analyses imply that a monocrystalline line can be obtained by chemically welding distinct nanocubes with the above-mentioned procedure. Figure 2B shows an overview TEM image of a bar composed of seven nanocubes after welding (see Figure S2, Supporting Information, for HRTEM), along with its SAED pattern (Figure 2C), which again indicates absence of grain boundaries and a [100]-oriented fcc lattice. Clearly, the epitaxial welding procedure is independent of the number of nanocubes that are welded and yields monocrystalline materials regardless of the scale. Additional TEM analysis of samples processed under the same conditions is reported in Figure S3 (Supporting Information). Our multiscale approach operates at the atomic scale during the chemical welding step but enables monocrystallinity at the full scale of the assembly.

Cathodoluminescence imaging spectroscopy (CL)[29] was employed to characterize the optical properties of assembled nanocubes before and after welding. **Figure 3**A shows the CL spectrum of a silver nanocube dimer before and after welding as well as the scattering spectrum for a welded dimer computed by finite difference time domain (FDTD) simulations, all for polarization parallel to the longitudinal axis. The experimental and calculated spectra for the welded structure are very similar, with one main peak at ≈750 nm due to the longitudinal dipolar plasmon mode of the dimer. Note that the difference in the line width of the CL data and FDTD simulations is less than 2%, suggesting that the welded structures exhibit optical constants equivalent to monocrystalline silver. The unwelded sample shows a completely different spectrum featuring a weak peak at 870 nm and a more intense feature at higher energy (peaking outside the spectral sensitivity range of our detector).

Figure 3B shows the 2D CL map of the welded dimer measured at 750 nm, using a 10×10 nm^2 grid. Figure 3C displays a time snapshot of the simulated amplitude of the z-component of the electric field calculated at 750 nm (in CL the electron beam couples to this z-component[30]). In both experiment and simulation, the signature of the dipolar mode can be clearly observed. This provides further evidence for our hypothesis that

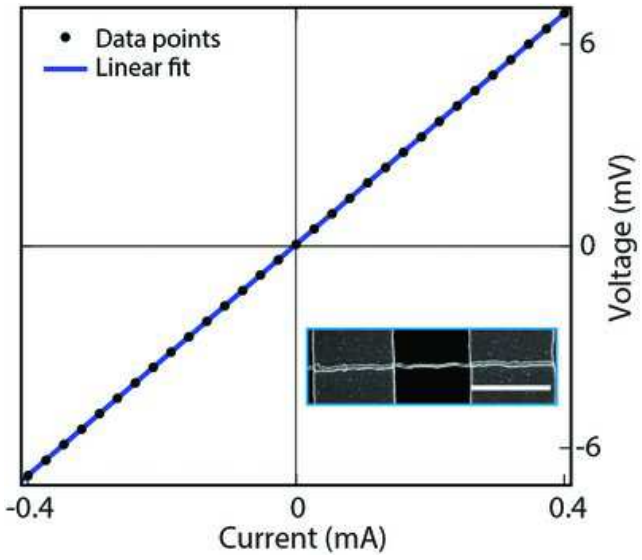

Figure 4. Electrical characterization of a 6 μm long welded line. A resistance of $R = 17\ \Omega$ is measured, which corresponds to a resistivity of $2 \times 10^{-8}\ \Omega$m. The inset shows an SEM image of the two internal contacts at which the voltage is measured. The scale bar is 2 μm.

after welding the nanocube subunits become electrically connected and behave as a true continuous material. This suggests that optical materials with properties close to theoretical ones can be realized from a simple solution process.

The DC conductivity of monocrystalline lines obtained from assembly and welding of silver nanocubes was characterized using a specially designed four-point probe geometry (see Figure S4, Supporting Information). **Figure 4** shows the current–voltage (I–V) characteristic of a 6 μm long line with a cross section of $85 \times 85\ nm^2$. The electric response is ohmic, with a resistance of 17 Ω, which corresponds to an intrinsic resistivity of $2.0 \times 10^{-8}\ \Omega$m. For this calculation, the full length of the bar was used (6 μm), which includes the metal contact width (2 μm each). According to previous literature on electrical characterization of Ag nanowires, the full contact width has to be taken into account to get accurate resistivity measurements.[31] The intrinsic resistivity of silver is $1.63 \times 10^{-8}\ \Omega$m at 300 K; if surface scattering is taken into account, an ideal silver line with the dimensions of our sample would have an intrinsic resistivity of $1.8 \times 10^{-8}\ \Omega$m (see Figure S5, Supporting Information), only 10% lower than the measured value. This indicates that grain boundary scattering does not play an important role and that the resistivity is determined by electron–phonon scattering, as in an ideal metal,[32] further supporting the epitaxial welding model. These findings are in accordance with other literature reports that studied the conductivity of quasi-monocrystalline (pentatwinned) Ag nanowires grown in solution with a one-step polyol process.[31]

We have presented a new versatile bottom-up method to obtain ultrahigh quality nanopatterned truly monocrystalline (no twinning) silver lines that uses epitaxy between aligned nanocubes instead of substrate epitaxy. The new method removes the substrate requirements of conventional epitaxial growth methods and opens up the possibility to create 1D, 2D, and 3D single-crystalline silver architectures. Following this first demonstration for silver, the same strategy should in principle be applicable to other metals or even semiconductors and dielectrics, further expanding the application range of the new method presented here. A key requirement for transferability to other materials is the ability to synthesize monodispersed nanocubes in solution, which has been demonstrated for many metals, semiconductors, and dielectrics including Cu, Au, Pd, Cu_2O, FeS_2, halide perovskites, oxide perovskites, piezoelectrics, and CeO_2 but so far not for III–V or group IV materials such as GaAs and Si. The major technical challenge will be to develop suitable chemical welding procedures for each new material. This may ultimately leverage the knowledge in nanocrystal synthesis and epitaxial core–shell growth to make monocrystalline materials at the macroscale.

Supporting Information

Supporting Information is available from the Wiley Online Library or from the author.

Acknowledgements

The work at AMOLF is part of the research program of the "Stichting voor Fundamenteel Onderzoek der Materie" (FOM), which was financially supported by the "Nederlandse Organisatie voor Wetenschappelijk Onderzoek" (NWO). This work was supported by the NWO VIDI grant (project number 14846) and by the European Research Council (Grant Agreements Nos. 337328, 683076, and 695343). B.S. and E.C.G. conceived the idea of the project. A.B. helped in developing the process and performed preliminary experiments. B.S. performed the nanocube synthesis, assembly and welding, the electrical measurements and the FDTD simulations. B.J.M.B. performed CL measurements, under the supervision of A.P. and S.Z.O. fabricated the Si_3N_4 membrane used for TEM measurements. M.A.H. performed the TEM characterization. B.S. wrote the paper. E.C.G. supervised the project. All authors contributed to the paper. A.P. is cofounder and coowner of Delmic BV, a startup company marketing a commercial product based on the cathodoluminescence system that was used in this work. The authors thank Dr. Wim Noorduin and Dr. Sarah Brittman for carefully reading the paper, Ricardo Struik for the artwork of Figure 1d, and Bob Drent for the realization of the silicon master used for PDMS patterning.

Conflict of Interest

The authors declare no conflict of interest.

Keywords

chemical welding, monocrystalline nanopatterns, nanocube assembly, silver nanostructures, solution phase homoepitaxy

Received: February 22, 2017
Revised: March 16, 2017
Published Online: MM DD, YYYY

[1] Y. J. Lu, J. Kim, H. Y. Chen, C. H. Wu, N. Dabidian, C. E. Sanders, C. Y. Wang, M. Y. Lu, B. H. Li, X. G. Qiu, W. H. Chang, L. J. Chen, G. Shvets, C. K. Shih, S. Gwo, *Science* **2012**, *337*, 450.
[2] Y. W. Wu, C. D. Zhang, N. M. Estakhri, Y. Zhao, J. Kim, M. Zhang, X. X. Liu, G. K. Pribil, A. Alu, C. K. Shih, X. Q. Li, *Adv. Mater.* **2014**, *26*, 6106.
[3] A. A. High, R. C. Devlin, A. Dibos, M. Polking, D. S. Wild, J. Perczel, N. P. de Leon, M. D. Lukin, H. Park, *Nature* **2015**, *522*, 192.
[4] D. Shi, V. Adinolfi, R. Comin, M. J. Yuan, E. Alarousu, A. Buin, Y. Chen, S. Hoogland, A. Rothenberger, K. Katsiev, Y. Losovyj, X. Zhang, P. A. Dowben, O. F. Mohammed, E. H. Sargent, O. M. Bakr, *Science* **2015**, *347*, 519.
[5] A. Polman, M. Knight, E. C. Garnett, B. Ehrler, W. C. Sinke, *Science* **2016**, *352*, aad4424.
[6] X. Sheng, C. A. Bower, S. Bonafede, J. W. Wilson, B. Fisher, M. Meitl, H. Yuen, S. D. Wang, L. Shen, A. R. Banks, C. J. Corcoran, R. G. Nuzzo, S. Burroughs, J. A. Rogers, *Nat. Mater.* **2014**, *13*, 593.
[7] B. O. Dabbousi, J. RodriguezViejo, F. V. Mikulec, J. R. Heine, H. Mattoussi, R. Ober, K. F. Jensen, M. G. Bawendi, *J. Phys. Chem. B* **1997**, *101*, 9463.
[8] X. G. Peng, M. C. Schlamp, A. V. Kadavanich, A. P. Alivisatos, *J. Am. Chem. Soc.* **1997**, *119*, 7019.
[9] S. E. Habas, H. Lee, V. Radmilovic, G. A. Somorjai, P. Yang, *Nat. Mater.* **2007**, *6*, 692.
[10] M. P. Boneschanscher, W. H. Evers, J. J. Geuchies, T. Altantzis, B. Goris, F. T. Rabouw, S. A. P. van Rossum, H. S. J. van der Zant, L. D. A. Siebbeles, G. Van Tendeloo, I. Swart, J. Hilhorst, A. V. Petukhov, S. Bals, D. Vanmaekelbergh, *Science* **2014**, *344*, 1377.
[11] B. Sciacca, S. A. Mann, F. D. Tichelaar, H. W. Zandbergen, M. A. van Huis, E. C. Garnett, *Nano Lett.* **2014**, *14*, 5891.
[12] J. J. De Yoreo, P. U. P. A. Gilbert, N. A. J. M. Sommerdijk, R. L. Penn, S. Whitelam, D. Joester, H. Z. Zhang, J. D. Rimer, A. Navrotsky, J. F. Banfield, A. F. Wallace, F. M. Michel, F. C. Meldrum, H. Colfen, P. M. Dove, *Science* **2015**, *349*, aaa6760.
[13] Z. J. Ning, X. W. Gong, R. Comin, G. Walters, F. J. Fan, O. Voznyy, E. Yassitepe, A. Buin, S. Hoogland, E. H. Sargent, *Nature* **2015**, *523*, 324.
[14] T. Kraus, L. Malaquin, H. Schmid, W. Riess, N. D. Spencer, H. Wolf, *Nat. Nanotechnol.* **2007**, *2*, 570.
[15] Y. G. Sun, Y. N. Xia, *Science* **2002**, *298*, 2176.
[16] A. Tao, P. Sinsermsuksakul, P. D. Yang, *Angew. Chem., Int. Ed.* **2006**, *45*, 4597.
[17] F. Dang, K. Mimura, K. Kato, H. Imai, S. Wada, H. Haneda, M. Kuwabara, *CrystEngComm* **2011**, *13*, 3878.
[18] H. A. Macpherson, C. R. Stoldt, *ACS Nano* **2012**, *6*, 8940.
[19] H. J. Yang, S. Y. He, H. L. Chen, H. Y. Tuan, *Chem. Mater.* **2014**, *26*, 1785.
[20] H. S. Chen, S. C. Wu, M. H. Huang, *Dalton Trans.* **2015**, *44*, 15088.
[21] L. Protesescu, S. Yakunin, M. I. Bodnarchuk, F. Krieg, R. Caputo, C. H. Hendon, R. X. Yang, A. Walsh, M. V. Kovalenko, *Nano Lett.* **2015**, *15*, 3692.
[22] Y. Cui, M. T. Bjork, J. A. Liddle, C. Sonnichsen, B. Boussert, A. P. Alivisatos, *Nano Lett.* **2004**, *4*, 1093.
[23] L. Malaquin, T. Kraus, H. Schmid, E. Delamarche, H. Wolf, *Langmuir* **2007**, *23*, 11513.
[24] A. Tao, P. Sinsermsuksakul, P. Yang, *Nat. Nanotechnol.* **2007**, *2*, 435.
[25] A. R. Tao, J. X. Huang, P. D. Yang, *Acc. Chem. Res.* **2008**, *41*, 1662.
[26] B. Sciacca, J. van de Groep, A. Polman, E. C. Garnett, *Adv. Mater.* **2016**, *28*, 905.
[27] Y. Nakagawa, H. Kageyama, Y. Oaki, H. Imai, *Langmuir* **2015**, *31*, 6197.
[28] K. Nakamura, Y. Nakagawa, H. Kageyama, Y. Oaki, H. Imai, *Langmuir* **2016**, *32*, 4066.
[29] T. Coenen, F. B. Arango, A. F. Koenderink, A. Polman, *Nat. Commun.* **2014**, *5*.
[30] F. J. G. de Abajo, *Rev. Mod. Phys.* **2010**, *82*, 209.
[31] M. M. Kolesnik, S. Hansel, T. Lutz, N. Kinahan, M. Boese, V. Krstic, *Small* **2011**, *7*, 2873.
[32] R. A. Matula, *J. Phys. Chem. Ref. Data* **1979**, *8*, 1147.

Q6

Q1 APT to AU: Please spell out the full first names of each author in the byline.

Q2 APT to AU: Please provide the highest academic title (Dr./Prof.) for all authors, where applicable.

Q3 APT to AU: If you have not returned the color cost confirmation form already, please email the completed form to the editorial office when you submit your proof corrections. This will confirm that you are willing to support the cost for color publication of the figures. Details about our color policies and a link to the form were included with your acceptance email. If you wish for your figures to be presented in grayscale, please email the editorial office to confirm this.

Q4 APT to AU: Please check expansion of CL.

Q5 APT to AU: Please provide the expansion of AMOLF and VIDI as these have been cited once in the article.

Q6 APT to AU: Please provide page number in ref. (29).